Energy-Efficient Federated Learning Over-the-Air with Perfect Amplitude Alignment Based on Magnitude-Scaled One-Bit Quantization

Junsuk Oh, Seonghun Hong, Donghyun Lee, Thwe Thwe Win, Hao Hoang Tran, Chunghyun Lee, Chihyun Song, Gahyun Kim, Seongjin Choi, and Sungrae Cho
School of Computer Science and Engineering, Chung-Ang University, Seoul 06974, Republic of Korea
Email: {jsoh, shhong, dhlee, ttwin, hhtran, chlee, chsong, ghkim, sjchoi}@uclab.re.kr, srcho@cau.ac.kr

***Abstract*—Federated learning (FL) typically suffers from the uplink exchange of high-dimensional updates, which yields a communication bottleneck. Thus, over-the-air computation enables FL to evolve into FL over-the-air (FLOA) through simultaneous aggregation. However, FLOA introduces gradient distortion from fading and noise, making the amplitude alignment (AA) crucial. Perfect AA (PAA) via full channel inversion (CI) ensures ideal aggregation, yet it risks unbounded power and suppresses small-magnitude gradient entries below the noise floor. To address this, we propose the magnitude-scaled one-bit analog aggregation with PAA (MOAA-PAA), coupled with truncated CI to cap power. The proposed design preserves both signs and the averaged magnitude, protects weak gradients, and retains identical alignment. Then, we analyze the convergence performance and discuss the energy efficiency of MOAA-PAA. In experiments, the proposed design shows improved trade-offs over baselines.**

***Index Terms*—Amplitude alignment, federated learning over-the-air, magnitude-scaled one-bit quantization, truncated channel inversion power control**

I. Introduction

Federated learning (FL) enables multiple devices to collaboratively train the global learning model without sharing raw data, preserving privacy and reducing traffic [1]–[3]. However, when many devices participate in wireless settings, repeated exchanges of high-dimensional updates (i.e., gradients) yield a severe uplink bottleneck that limits scalability and efficiency [4]. To address this, over-the-air computation (OAC) has been integrated into FL, appearing as FL over-the-air (FLOA) [5], [6]. FLOA exploits waveform superposition to enable simultaneous transmissions and high communication efficiency, but suffers from gradient distortion from fading and noise.

Therefore, power control with amplitude alignment (AA) has become central to preserving the ideal aggregated gradient. Perfect AA (PAA) performs identical amplitude scaling-based full channel inversion (CI); that is, all gradients arrive at the parameter server (PS) as identical amplitude, which enables fading-driven error-free aggregation and ideal learning theoretically [5]–[8]. However, PAA's drawback is the unbounded transmit power under deep fading. This motivates imperfect AA (IAA), in which devices use different amplitude scaling, tolerating misalignment to avoid excessive power and improve robustness [9]–[12].

Nonetheless, in terms of the learning theory, PAA remains attractive, as it enables an ideal aggregation and preserves the integrity of the global gradient. Thus, some PAA-based works apply a truncated CI (TCI), silencing devices in deep fading to cap transmit power while keeping PAA's learning benefits [5], [7]. However, another drawback of PAA arises from its amplitude scaling structure. Because devices compensate for their fading differently, small-magnitude gradients may sink below the noise floor at PS even when an identical amplitude scaling is used. In contrast, large-magnitude gradients survive, potentially destabilizing learning. To fix this, some auxiliary methods are utilized: normalization boosts weak gradients but can also amplify noise upon denormalization [5], [6]. One-bit quantization avoids that amplification by fixing magnitudes to one, but it discards magnitude information [7], [8].

That is, the conventional auxiliary methods address another drawback of PAA through their unique approaches, but they face new shortcomings. To navigate these trade-offs, we introduce the magnitude-scaled one-bit (MO) quantization as an auxiliary approach. Then, we propose MO analog aggregation with PAA (MOAA-PAA). It avoids both complete information loss and noise amplification. Unlike prior one-bit schemes that intentionally discard magnitude to prevent noise amplification, the proposed design preserves sign information while recovering the averaged magnitude, and it further adopts TCI to avoid the unbounded transmit power required by strict PAA.

II. System Model

For the wireless FL, the network consists of a single PS and K devices. Device $k \in [K] \triangleq \mathcal{K}$ has its local dataset $\mathcal{D}_k$ with $D = |\mathcal{D}_k|$, $\forall k$. Thus, device k trains the learning model using $\mathcal{D}_k$ and derives the local loss function $\mathsf{F}_k(\cdot)$ as follows:

$$\mathsf{F}_k(\mathbf{w}) = \frac{1}{D} \sum_{d \in \mathcal{D}_k} \mathsf{F}_{k,d}(\mathbf{w}), \tag{1}$$

where $\mathbf{w} \in \mathbb{R}^S$ is a parameter vector, and $\mathsf{F}_{k,d}(\cdot)$ is a sample-wise loss function. Based on all local loss functions, the global loss function is defined as $\mathsf{F}(\mathbf{w}) = \sum_{k \in \mathcal{K}} \mathsf{F}_k(\mathbf{w})/K$. The goal of FL is to find an optimal parameter vector $\mathbf{w}^\star$ as

$$\mathbf{w}^\star = \arg\min_{\mathbf{w}} \mathsf{F}(\mathbf{w}). \tag{2}$$

To find $\mathbf{w}^\star$, the FL framework is employed in a distributed manner. In communication round $t \in [T]$, device k derives the local gradient vector $\mathbf{g}_k^t \in \mathbb{R}^S$ as follows:

$$\mathbf{g}_k^t = \frac{1}{D} \sum_{d \in \mathcal{D}_k} \nabla \mathsf{F}_{k,d}(\mathbf{w}^t), \tag{3}$$

where $\nabla \mathsf{F}_{k,d}(\cdot)$ is the sample-wise gradient vector. Thus, the PS derives the global gradient vector as $\mathbf{g}^t = \sum_{k \in \mathcal{K}} \mathbf{g}_k^t / K$, which denotes $\nabla \mathsf{F}(\mathbf{w}^t)$. Then, after the PS broadcasts this to all devices, the parameter vector $\mathbf{w}^t$ is updated as

$$\mathbf{w}^{t+1} = \mathbf{w}^t - \lambda \mathbf{g}^t, \tag{4}$$

where λ is the learning rate. This process is iterated until the maximum round T is reached or convergence is achieved.

III. Proposed Design

First, we introduce MO quantization, which preserves both signs and the averaged magnitude. In round t, device k derives the magnitude scaling factor u_k^t as

$$u_k^t = \|\mathbf{g}_k^t\|_1 / S, \tag{5}$$

and derives the quantized gradient vector $\mathbf{q}_k^t \in \mathbb{R}^S$ as

$$q_{k,s}^t = \begin{cases} +1, & g_{k,s}^t \geq 0, \\ -1, & \text{otherwise}, \end{cases} \tag{6}$$

where $s \in [S]$. Then, for the aggregation in the PS, device k transmits the channel input vector $\mathbf{x}_k^t$, defined as

$$\mathbf{x}_k^t = u_k^t \mathbf{q}_k^t. \tag{7}$$

Since all $\{\mathbf{x}_k^t\}_{k \in \mathcal{K}}$ are transmitted in an analog manner, the channel output vector $\mathbf{y}^{t,a}$ is represented as

$$\mathbf{y}^{t,a} = \sum_{k \in \mathcal{K}} h_k^t p_k^{t,a} \mathbf{x}_k^t + \mathbf{z}^t, \tag{8}$$

where $a \in \{\mathrm{Paa}, \mathrm{Iaa}\}$ is the type of amplitude alignment, and $h_k^t \sim \mathcal{CN}(0,1)$ denotes channel coefficient between device k and PS. For simplicity, we assumed the perfect uplink channel state information and block fading. In addition, $p_k^{t,a} \geq 0$ and $\mathbf{z}^t \sim \mathcal{CN}(0, \sigma^2)$ denote the transmit power and additive white Gaussian noise (AWGN) vector, respectively.

In each round t, the transmit power $p_k^{t,a}$ should be inverted to the corresponding channel coefficient h_k^t, and it is subject to a long-term transmit power constraint as

$$\mathbb{E}[|p_k^{t,a} x_{k,s}^t|^2] \leq P_0. \tag{9}$$

The full CI is infeasible because some channels encounter deep fading. Thus, we adopt TCI that control $p_k^{t,a}$ as

$$p_k^{t,a} = \frac{1_\delta(|h_k^t|^2)(h_k^t)^*}{|h_k^t|^2} \times \begin{cases} b_0^t, & a = \mathrm{Paa}, \\ b_k^t, & \text{otherwise}, \end{cases} \tag{10}$$

where $1_\delta(|h_k^t|^2)$ is the indicator function in which 1 if $|h_k^t|^2 \geq \delta$, otherwise 0. In addition, b_0^t and b_k^t are the amplitude scaling factors for PAA and IAA, respectively, to satisfy the constraint (9). Given $\mathbf{y}^{t,a}$, the PS derive $\mathbf{v}^{t,a}$ as the estimation of $\mathbf{x}^t = \sum_{k \in \mathcal{K}} \mathbf{x}_k^t / K$, and broadcast it to all devices to update

$$\mathbf{w}^{t+1} = \mathbf{w}^t - \lambda \mathbf{v}^{t,a}. \tag{11}$$

A. Amplitude Alignment

For PAA implementation, by substituting (7) and (10) into $x_{k,s}^t$ and $p_k^{t,a}$, respectively, the constraint (9) is rewritten as

$$\mathbb{E}\left[\frac{1_\delta(|h_k^t|^2)|b_0^t|^2 |u_k^t|^2}{|h_k^t|^2}\right] = \mathsf{E}_1(\delta)(b_0^t)^2 (u_k^t)^2 \leq P_0, \tag{12}$$

that is,

$$b_0^t \leq \sqrt{\frac{P_0}{(u_k^t)^2 \mathsf{E}_1(\delta)}}, \tag{13}$$

where $\mathsf{E}_1(\delta) = \int_\delta^\infty \frac{1}{\tau} e^{-\tau} d\tau$ is the exponential integral function. The higher u_k^t's devices need their lower transmit power to achieve PAA with the lower u_k^t's devices. Thus, according to $\{u_k^t\}_{k \in \mathcal{K}}$ known in advance before transmission, PS set

$$b_0^t = \sqrt{\frac{P_0}{(u_{\max}^t)^2 \mathsf{E}_1(\delta)}}, \tag{14}$$

where $u_{\max}^t = \max_k \{u_k^t\}$. By substituting PAA case's (10) into (8), the channel output vector $\mathbf{y}^{t,\mathrm{Paa}}$ is written as

$$\mathbf{y}^{t,\mathrm{Paa}} = \sum_{k \in \mathcal{K}} 1_\delta(|h_k^t|^2) b_0^t \mathbf{x}_k^t + \mathbf{z}^t. \tag{15}$$

Upon this, the PS extracts the real component and then derives the estimated $\mathbf{x}^t$ as

$$\begin{aligned} \mathbf{v}^{t,\mathrm{Paa}} = \frac{\mathbf{y}_{\mathrm{re}}^{t,\mathrm{Paa}}}{K b_0^t} &= \frac{1}{K} \sum_{k \in \mathcal{H}^t} \mathbf{x}_k^t + \frac{\mathbf{z}_{\mathrm{re}}^t}{K b_0^t}, \\ &= \frac{1}{K} \sum_{k \in \mathcal{H}^t} \mathbf{x}_k^t + \mathbf{n}^{t,\mathrm{Paa}}, \end{aligned} \tag{16}$$

where $\mathcal{H}^t = \{k \in \mathcal{K} : |h_k^t|^2 \geq \delta\}$, and $\mathbf{n}^{t,\mathrm{Paa}}$ represents the noise-driven error vector.

To demonstrate the performance of PAA, we also implement IAA as a comparison power control design by referring to [9]. It doesn't matter if each device is not aligned with the other devices; thus, each device sets

$$b_k^t = \sqrt{\frac{P_0}{(u_k^t)^2 \mathsf{E}_1(\delta)}}. \tag{17}$$

Similarly, IAA case's $\mathbf{y}^{t,\mathrm{Iaa}}$ and $\mathbf{v}^{t,\mathrm{Iaa}}$ are derived as

$$\mathbf{y}^{t,\mathrm{Iaa}} = \sum_{k \in \mathcal{K}} 1_\delta(|h_k^t|^2) b_k^t \mathbf{x}_k^t + \mathbf{z}^t, \tag{18}$$

$$\begin{aligned} \mathbf{v}^{t,\mathrm{Iaa}} = \frac{\mathbf{y}_{\mathrm{re}}^{t,\mathrm{Iaa}}}{K b_{\mathrm{avg}}^t} &= \frac{1}{K b_{\mathrm{avg}}^t} \sum_{k \in \mathcal{H}^t} b_k^t \mathbf{x}_k^t + \frac{\mathbf{z}_{\mathrm{re}}^t}{K b_{\mathrm{avg}}^t} \\ &= \frac{1}{K} \sum_{k \in \mathcal{H}^t} \mathbf{x}_k^t + \frac{1}{K} \sum_{k \in \mathcal{K}} \mathbf{m}_k^t + \mathbf{n}^{t,\mathrm{Iaa}}, \end{aligned} \tag{19}$$

where $b_{\mathrm{avg}}^t = \sum_{k \in \mathcal{K}} b_k^t / K$ derived by the PS based on amplitude scaling factors additionally transmitted after the transmission of channel input vectors, and $\mathbf{m}_k^t$ is the misalignment-driven error vector, defined as

$$\mathbf{m}_k^t = 1_\delta(|h_k^t|^2) \left(\frac{b_k^t}{b_{\mathrm{avg}}^t} - 1\right) \mathbf{x}_k^t. \tag{20}$$

B. Energy Consumption

For OAC, each entry of $\mathbf{x}_k^t$ is modulated as a single analog symbol; that is, the total of S analog symbols is transmitted. Thus, we consider the LTE uplink system where one resource block (RB) spans two slots, each slot contains $\psi_0 = 7$ symbols (i.e., 14 symbols per RB) with duration $\phi_{\text{slot}} = 0.5$ ms [12]. The transmission latency R is expressed as

$$R = 2\phi_{\text{slot}} \left\lceil \frac{S}{2\psi_0} \right\rceil. \tag{21}$$

According to (21), the energy consumption per round of PAA is expected to be

$$\begin{aligned} \sum_{k\in\mathcal{K}} \mathbb{E}\left[\frac{1_\delta(|h_k^t|^2)|u_k^t|^2 P_0 R}{|h_k^t|^2 |u_{\max}^t|^2 \mathsf{E}_1(\delta)} \right] &= \frac{P_0 R}{(u_{\max}^t)^2} \sum_{k\in\mathcal{K}} (u_k^t)^2 \\ &= j^t K P_0 R, \end{aligned} \tag{22}$$

where $j^t = \frac{1}{K}\sum_{k\in\mathcal{K}} (u_k^t)^2/(u_{\max}^t)^2$. Furthermore, the energy consumption per round of IAA is expected to be

$$\sum_{k\in\mathcal{K}} \mathbb{E}\left[\frac{1_\delta(|h_k^t|^2) P_0 R}{|h_k^t|^2 \mathsf{E}_1(\delta)} \right] = K P_0 R. \tag{23}$$

Since it is typically $j^t \leq 1$, the energy consumption per round of PAA is expected to be lower than that of IAA.

IV. Convergence Analysis

This section characterizes the effects of MOAA-PAA/IAA on the FLOA system by analyzing its convergence rate.

A. Standard Assumptions

For facilitating convergence analysis, we made the standard assumptions regarding the loss function and gradient vector.

Assumption 1. *(Loss Function Bound):* The global loss function $\mathsf{F}(\cdot)$ is lower bounded by an optimal parameter vector $\mathbf{w}^\star$ for the given $\mathbf{w}$, that is,

$$\mathsf{F}(\mathbf{w}) \geq \mathsf{F}(\mathbf{w}^\star), \quad \forall \mathbf{w} \in \mathbb{R}^S. \tag{24}$$

Assumption 2. *(Smoothness and Lipschitz Continuity):* The global loss function $\mathsf{F}(\cdot)$ is L-smooth and the corresponding $\nabla\mathsf{F}(\cdot)$ is L-Lipschitz continuous, that is,

$$\begin{aligned} &|\mathsf{F}(\mathbf{w}') - \mathsf{F}(\mathbf{w}) - (\mathbf{w}' - \mathbf{w})^\top \nabla\mathsf{F}(\mathbf{w})| \\ &\leq \frac{L}{2}\|\mathbf{w}' - \mathbf{w}\|_2^2, \quad \forall \mathbf{w}', \mathbf{w} \in \mathbb{R}^S, \end{aligned} \tag{25}$$

where L is a non-negative constant.

Assumption 3. *(Local Gradient Vector Bound):* There exists a constant $G > 0$ such that the local gradient vector $\mathbf{g}_k \in \mathbb{R}^S$ is bounded by

$$\|\mathbf{g}_k\|_2^2 \leq G^2, \quad \forall k. \tag{26}$$

B. Main Results

Based on the assumptions, we provided the expected convergence rate of the proposed MOAA-PAA/IAA as a closed-form expression. First, we derived **Lemma 1** to describe the upper bound of the magnitude scaling factor.

Lemma 1. Under **Assumption 3**, the magnitude scaling factor u_k^t is bounded by

$$(u_k^t)^2 \leq G^2/S, \quad \forall t, k, \tag{27}$$

and then there exist a constant $\xi \in (0, 1)$ such that

$$\frac{1}{K}\sum_{k\in\mathcal{K}} (u_k^t)^2 \leq \xi G^2/S, \quad \forall t. \tag{28}$$

Proof: See Appendix A. ∎

Next, we derived **Lemmas 2-5** to present the compression, misalignment-driven, and noise-driven errors.

Lemma 2. Upon MO quantization, TCI, and PAA, the compression error vector $\mathbf{c}_k^t$ is defined as

$$\mathbf{c}_k^t = \mathbf{g}_k^t - 1_\delta(|h_k^t|^2)\mathbf{x}_k^t, \tag{29}$$

and it is bounded by

$$\mathbb{E}\|\mathbf{c}_k^t\|_2^2 \leq (1 - e^{-\delta}/S)G^2, \tag{30}$$

under **Assumption 3** and **Lemma 1**.

Proof: See Appendix B. ∎

Lemma 3. Upon MO quantization, TCI, and IAA, the error vector $\mathbf{o}_k^t$ by compression and misalignment is defined as

$$\mathbf{o}_k^t = \mathbf{c}_k^t - \mathbf{m}_k^t = \mathbf{g}_k^t - 1_\delta(|h_k^t|^2)\frac{b_k^t}{b_{\text{avg}}^t}\mathbf{x}_k^t, \tag{31}$$

and it is bounded by

$$\mathbb{E}\|\mathbf{o}_k^t\|_2^2 \leq (1 + \xi e^{-\delta})G^2, \tag{32}$$

under **Assumption 3** and **Lemma 1**.

Proof: See Appendix C. ∎

Lemma 4. Based on (14), (16), and **Lemma 1**, PAA case's noise-driven error vector $\mathbf{n}^{t,\text{Paa}}$ is bounded by

$$\begin{aligned} \mathbb{E}\|\mathbf{n}^{t,\text{Paa}}\|_2^2 = \mathbb{E}\left\| \frac{\mathbf{z}_{\text{re}}^t}{K b_0^t} \right\|_2^2 &= \frac{\sigma^2 S \mathsf{E}_1(\delta)(u_{\max}^t)^2}{2P_0 K^2} \\ &\leq \frac{\sigma^2 G^2 \mathsf{E}_1(\delta)}{2P_0 K^2}, \end{aligned} \tag{33}$$

which completes the proof. ∎

Lemma 5. Based on (17), (19), Cauchy-Schwarz inequality, Jensen's inequality, and **Lemma 1**, IAA case's noise-driven error vector $\mathbf{n}^{t,\text{Iaa}}$ is bounded by

$$\begin{aligned} \mathbb{E}\|\mathbf{n}^{t,\text{Iaa}}\|_2^2 = \mathbb{E}\left\| \frac{\mathbf{z}_{\text{re}}^t}{K b_{\text{avg}}^t} \right\|_2^2 &= \frac{\sigma^2 S \mathsf{E}_1(\delta)}{2P_0(\sum_{k\in\mathcal{K}} 1/u_k^t)^2} \\ &\leq \frac{\sigma^2 S \mathsf{E}_1(\delta)}{2P_0 K^3} \sum_{k\in\mathcal{K}} (u_k^t)^2 \\ &\leq \frac{\xi\sigma^2 G^2 \mathsf{E}_1(\delta)}{2P_0 K^2}, \end{aligned} \tag{34}$$

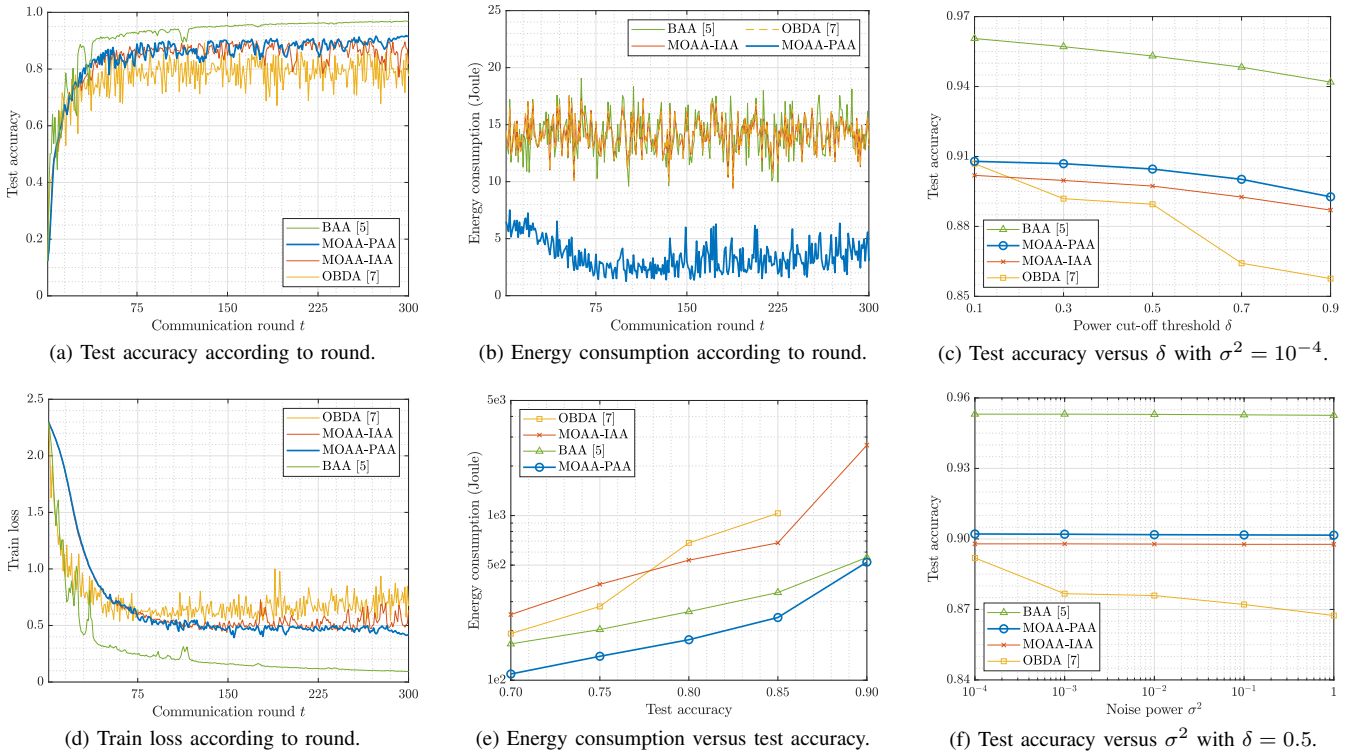

(a) Test accuracy according to round.
(b) Energy consumption according to round.
(c) Test accuracy versus δ with $\sigma^2 = 10^{-4}$.
(d) Train loss according to round.
(e) Energy consumption versus test accuracy.
(f) Test accuracy versus σ^2 with $\delta = 0.5$.

Fig. 1: Evaluation of learning performance, energy efficiency, and uncertainty robustness.

which completes the proof. ■

Lastly, we derived to delineate the convergence rates of the proposed MOAA-PAA/IAA in **Theorems 1**-**2**.

Theorem 1. Based on **Lemmas 2**, **4**, and **Assumptions 1**-**2**, the convergence rate of MOAA-PAA satisfies

$$\frac{1}{T}\sum_{t=1}^{T}\|\nabla \mathsf{F}(\mathbf{w}^t)\|_2^2 \leq \frac{2(\mathsf{F}(\mathbf{w}^1)-\mathsf{F}(\mathbf{w}^\star))}{\lambda T} + \frac{\sigma^2 G^2 \mathsf{E}_1(\delta)}{2P_0K^2} + (1-e^{-\delta}/S)G^2. \tag{35}$$

The right-hand side (RHS) upper-bounds the average stationary measure by the optimization term decaying with T and λ, the weighted noise-driven error (WNE) term decreasing with larger P_0 and K, and the weighted compression error (WCE) term governed by δ and S.

Proof: See Appendix D. ■

Theorem 2. Based on **Lemmas 3**, **5**, and **Assumptions 1**-**2**, the convergence rate of MOAA-IAA satisfies

$$\frac{1}{T}\sum_{t=1}^{T}\|\nabla \mathsf{F}(\mathbf{w}^t)\|_2^2 \leq \frac{2(\mathsf{F}(\mathbf{w}^1)-\mathsf{F}(\mathbf{w}^\star))}{\lambda T} + \frac{\xi\sigma^2 G^2 \mathsf{E}_1(\delta)}{2P_0K^2} + (1+\xi e^{-\delta})G^2. \tag{36}$$

Compared with **Theorem 1**, the upper-bound in the RHS has the same optimization term. However, its WNE is smaller than that of the PAA case, whereas its WCE term is larger.

Proof: See Appendix E. ■

From **Theorems 1** and **2**, MOAA-PAA converges faster and achieves better performance than MOAA-IAA theoretically if the WNE term is negligibly small, since the PAA case has a smaller WCE term than the IAA case. Otherwise, MOAA-IAA may become better than MOAA-PAA.

V. Experimental Results

In this section, we evaluate the learning performance, energy efficiency, and uncertainty robustness of the proposed MOAA-PAA. We considered $K = 100$ devices with the learning rate $\lambda = 0.5$. Moreover, we set $T = 300$, $P_0 = 10$ mW, $\sigma^2 = 10^{-4}$ mW, and $\delta = 0.5$. We compared the proposed MOAA-PAA with the MOAA-IAA, as well as broadband analog aggregation (BAA) [5] and one-bit broadband digital aggregation (OBDA) [7], which adopt normalization and unscaled one-bit quantization, respectively, as auxiliary methods. As an application, we considered image classification with the MNIST dataset, which consists of black-and-white handwritten digits from 0 to 9, comprising $60,000$ training samples and $10,000$ test samples. For 100 devices, non-i.i.d. partitioning sorts training samples by their label, divides into 200 shards, each 300 samples, and assigns each device two shards [1]. Then, we implemented the multilayer perceptron with $S = 199,210$ as a classifier [1]. The considered FLOA setup maps to an ICT deployment in which the PS runs on an edge server, and devices are mobile equipment or IoT endpoints, potentially connected via an IoT gateway that performs OAC. Therefore, the proposed MOAA-PAA is lightweight for resource-limited devices.

Figs. 1(a) and 1(d) plot test accuracy and train loss according to round, respectively. BAA and OBDA achieved the best performance with the fastest convergence and the worst performance with the slowest convergence, respectively. This is because BAA retains the magnitude information, while OBDA discards it. Furthermore, MOAA-IAA achieved better performance than OBDA, since it retains the averaged magnitude information. On the other hand, the proposed MOAA-PAA seeks identical alignment of the simultaneously transmitted gradients, achieving better performance than MOAA-IAA.

Fig. 1(b) plots the energy consumption according to round. As observed theoretically, MOAA-PAA consumes less energy per round than MOAA-IAA. Furthermore, BAA and OBDA show energy consumption similar to that of MOAA-IAA. As shown in 1(e), which plots the trade-off between energy consumption and test accuracy, the energy consumption of OBDA increased dramatically if test accuracy increased, resulting in the worst trade-off. It also failed to achieve a test accuracy of 0.9. MOAA-IAA achieved 0.9 test accuracy, but still showed a bad trade-off. In addition, BAA outperformed these. On the other hand, MOAA-PAA showed the best trade-off, achieving 0.9 test accuracy with reduced energy consumption by 80.5% and 6.3% compared to MOAA-IAA and BAA, respectively.

In Figs. 1(c) and 1(f), we compared the MOAA-PAA/IAA with other baselines in terms of the trade-offs between test accuracy with power cut-off threshold δ or noise power σ^2. For all designs, as the participation rate decreased with increasing δ or gradient distortion became more severe with increasing σ^2, the test accuracy reduced. Then, we showed the robustness of the proposed designs by comparing the test accuracy with different δ or σ^2. When σ^2 increases from 0.1 to 0.9 or σ^2 increases from 10^{-4} to 1, the test accuracy of MOAA-PAA decreases only about 0.015 or 0.0004, respectively, and it can be seen that it is more robust than both BAA and OBDA. On the other hand, MOAA-IAA showed slightly better robustness than the PAA case, with a 0.014 or 0.0002 decrease in test accuracy, respectively. This is because the adverse effect of the misalignment decreases as the participation rate drops, and it is theoretically less affected by noise than in the PAA case. Nevertheless, the difference in test accuracy decrease between MOAA cases is negligible.

VI. Conclusion

We tackled FLOA's core trade-off between identical alignment, learning performance, and energy efficiency; the proposed MOAA-PAA preserves signs and averaged magnitude, protects weak gradients from noise-floor erasure, and caps transmit power while retaining PAA's aggregation benefits. In both analysis and experiments, we demonstrate a better energy–accuracy trade-off than the IAA case and other PAA-based FLOA baselines, and derive closed-form convergence guarantees under standard smoothness with bounded transmit power. Extensive evaluations across power cut-off thresholds and noise levels further corroborate the theoretical insights and confirm consistent gains in both test accuracy and energy efficiency. Future work will extend the framework to partial participation and time-varying channels under non-ideal wireless conditions, such as imperfect CSI and heterogeneous devices, and validate generality on more complex datasets.

Appendix

A. Proof of *Lemma 1*

By **Assumption 3** and Cauchy-Schwarz inequality,

$$(u_k^t)^2 = \|\mathbf{g}_k^t\|_1^2/S^2 \le \|\mathbf{g}_k^t\|_2^2/S \le G^2/S, \quad \forall t,k. \tag{37}$$

Their average is bounded by $\sum_{k\in\mathcal{K}}(u_k^t)^2/K \le G^2/S$, that is, it can be denoted in proportional form as

$$\frac{1}{K}\sum_{k\in\mathcal{K}}(u_k^t)^2 = \frac{i^t G^2}{S}, \tag{38}$$

for some coefficient $i^t \in (0,1)$ in each round t. There exist a uniform margin $0 < \zeta \le 1 - i^t$ such that

$$\frac{1}{K}\sum_{k\in\mathcal{K}}(u_k^t)^2 \le (1-\zeta)\frac{G^2}{S}, \quad \forall t. \tag{39}$$

Then, by defining $\xi = 1 - \zeta$, we complete the proof. ∎

B. Proof of *Lemma 2*

Using (29) and $\mathbb{E}[1_\delta(|h_k^t|^2)] = \mathsf{Pr}(|h_k^t|^2 \ge \delta) = e^{-\delta}$,

$$\begin{aligned}\|\mathbf{c}_k^t\|_2^2 &= \|\mathbf{g}_k^t - 1_\delta(|h_k^t|^2)\mathbf{x}_k^t\|_2^2 \\ &= \|\mathbf{g}_k^t\|_2^2 - 21_\delta(|h_k^t|^2)\mathbf{g}_k^{t\top}\mathbf{x}_k^t + 1_\delta(|h_k^t|^2)\|\mathbf{x}_k^t\|_2^2. \end{aligned}\tag{40}$$

By (5), (6), (7), ℓ_1-ℓ_2 norm inequality, and **Assumption 3**,

$$\begin{aligned}\mathbb{E}\|\mathbf{c}_k^t\|_2^2 &= \|\mathbf{g}_k^t\|_2^2 - 2e^{-\delta}\mathbf{g}_k^{t\top}\mathbf{x}_k^t + e^{-\delta}\|\mathbf{x}_k^t\|_2^2 \\ &= \|\mathbf{g}_k^t\|_2^2 - 2e^{-\delta}u_k^t\|\mathbf{g}_k^t\|_1 + Se^{-\delta}(u_k^t)^2 \\ &= \left(1 - \frac{e^{-\delta}\|\mathbf{g}_k^t\|_1^2}{S\|\mathbf{g}_k^t\|_2^2}\right)\|\mathbf{g}_k^t\|_2^2 \\ &\le (1 - e^{-\delta}/S)\|\mathbf{g}_k^t\|_2^2 \\ &\le (1 - e^{-\delta}/S)G^2. \end{aligned}\tag{41}$$

Then, we complete the proof. ∎

C. Proof of *Lemma 3*

Using (6), (7), (17), Cauchy–Schwarz inequality, Jensen's inequality, **Lemma 1**, and **Assumption 3**,

$$\begin{aligned}\mathbb{E}\|\mathbf{o}_k^t\|_2^2 &= \mathbb{E}\left\|\mathbf{g}_k^t - 1_\delta(|h_k^t|^2)\frac{b_k^t}{b_{\text{avg}}^t}\mathbf{x}_k^t\right\|_2^2 \\ &= \mathbb{E}\left\|\mathbf{g}_k^t - \frac{1_\delta(|h_k^t|^2)K\mathbf{q}_k^t}{\sum_{k'\in\mathcal{K}}1/u_{k'}^t}\right\|_2^2 \\ &\le \|\mathbf{g}_k^t\|_2^2 + \frac{\mathbb{E}[1_\delta(|h_k^t|^2)]SK^2}{(\sum_{k'\in\mathcal{K}}1/u_{k'}^t)^2} \\ &\le \|\mathbf{g}_k^t\|_2^2 + \frac{Se^{-\delta}}{K}\sum_{k'\in\mathcal{K}}(u_{k'}^t)^2 \\ &\le (1 + \xi e^{-\delta})G^2. \end{aligned}\tag{42}$$

Then, we complete the proof. ∎

D. Proof of Theorem 1

Based on (16) and (29), the PAA case's update rule (11) is represented as

$$\begin{aligned}\mathbf{w}^{t+1} &= \mathbf{w}^t - \lambda \mathbf{v}^{t,\mathrm{Paa}} \\ &= \mathbf{w}^t - \frac{\lambda}{K}\sum_{k\in\mathcal{H}^t}\mathbf{x}_k^t - \lambda \mathbf{n}^{t,\mathrm{Paa}} \\ &= \mathbf{w}^t - \lambda \mathbf{g}^t + \lambda \mathbf{c}^t - \lambda \mathbf{n}^{t,\mathrm{Paa}}, \end{aligned} \tag{43}$$

where $\mathbf{c}^t = \sum_{k\in\mathcal{K}} \mathbf{c}_k^t/K$. By **Assumption 2**,

$$\begin{aligned}&\mathbb{E}[\mathsf{F}(\mathbf{w}^{t+1})] - \mathsf{F}(\mathbf{w}^t) \\ &\le \mathbb{E}[\mathbf{w}^{t+1} - \mathbf{w}^t]^\top \nabla \mathsf{F}(\mathbf{w}^t) + \frac{L}{2}\mathbb{E}\|\mathbf{w}^{t+1} - \mathbf{w}^t\|_2^2 \\ &= \lambda(1-\lambda L)\mathbb{E}[\mathbf{c}^t - \mathbf{n}^{t,\mathrm{Paa}}]^\top \nabla \mathsf{F}(\mathbf{w}^t) \\ &\quad + \frac{\lambda^2 L}{2}\mathbb{E}\|\mathbf{c}^t - \mathbf{n}^{t,\mathrm{Paa}}\|_2^2 - \lambda\left(1 - \frac{\lambda L}{2}\right)\|\nabla \mathsf{F}(\mathbf{w}^t)\|_2^2 \\ &= \frac{\lambda}{2}\mathbb{E}\|\mathbf{c}^t - \mathbf{n}^{t,\mathrm{Paa}}\|_2^2 - \frac{\lambda}{2}\left\|\nabla \mathsf{F}(\mathbf{w}^t)\right\|_2^2 \\ &= \frac{\lambda}{2}\mathbb{E}\|\mathbf{c}^t\|_2^2 + \frac{\lambda}{2}\mathbb{E}\|\mathbf{n}^{t,\mathrm{Paa}}\|_2^2 - \frac{\lambda}{2}\left\|\nabla \mathsf{F}(\mathbf{w}^t)\right\|_2^2 \\ &\le \frac{\lambda}{2K}\sum_{k\in\mathcal{K}}\mathbb{E}\|\mathbf{c}_k^t\|_2^2 + \frac{\lambda}{2}\mathbb{E}\|\mathbf{n}^{t,\mathrm{Paa}}\|_2^2 - \frac{\lambda}{2}\left\|\nabla \mathsf{F}(\mathbf{w}^t)\right\|_2^2, \end{aligned} \tag{44}$$

where $L = 1/\lambda$ for a simpler expression without compromising generality. Then, according to **Assumption 1**, **Lemmas 2**, and **4**, we rearrange the terms and take the average over t on both sides as follows:

$$\begin{aligned}\frac{1}{T}\sum_{t=1}^{T}\|\nabla \mathsf{F}(\mathbf{w}^t)\|_2^2 \le \frac{2(\mathsf{F}(\mathbf{w}^1) - \mathsf{F}(\mathbf{w}^\star))}{\lambda T} + \frac{\sigma^2 G^2 \mathsf{E}_1(\delta)}{2P_0K^2} \\ + (1 - e^{-\delta}/S)G^2, \end{aligned} \tag{45}$$

which completes the proof. ∎

E. Proof of Theorem 2

Based on (19), (29), and (31), the IAA case's update rule (11) is represented as

$$\begin{aligned}\mathbf{w}^{t+1} &= \mathbf{w}^t - \lambda \mathbf{v}^{t,\mathrm{Iaa}} \\ &= \mathbf{w}^t - \frac{\lambda}{K}\sum_{k\in\mathcal{H}^t}\mathbf{x}_k^t - \lambda \mathbf{m}^t - \lambda \mathbf{n}^{t,\mathrm{Iaa}} \\ &= \mathbf{w}^t - \lambda \mathbf{g}^t + \lambda \mathbf{c}^t - \lambda \mathbf{m}^t - \lambda \mathbf{n}^{t,\mathrm{Iaa}} \\ &= \mathbf{w}^t - \lambda \mathbf{g}^t + \lambda \mathbf{o}^t - \lambda \mathbf{n}^{t,\mathrm{Iaa}}, \end{aligned} \tag{46}$$

where $\mathbf{m}^t = \sum_{k\in\mathcal{K}} \mathbf{m}_k^t/K$, and $\mathbf{o}^t = \sum_{k\in\mathcal{K}} \mathbf{o}_k^t/K$. Then, identical to (44), but by replacing $\mathbf{n}^{t,\mathrm{Paa}}$ and $\mathbf{c}^t$ with $\mathbf{n}^{t,\mathrm{Iaa}}$ and $\mathbf{o}^t$, respectively,

$$\begin{aligned}&\mathbb{E}[\mathsf{F}(\mathbf{w}^{t+1})] - \mathsf{F}(\mathbf{w}^t) \\ &\le \frac{\lambda}{2K}\sum_{k\in\mathcal{K}}\mathbb{E}\|\mathbf{o}_k^t\|_2^2 + \frac{\lambda}{2}\mathbb{E}\|\mathbf{n}^{t,\mathrm{Iaa}}\|_2^2 - \frac{\lambda}{2}\left\|\nabla \mathsf{F}(\mathbf{w}^t)\right\|_2^2, \end{aligned} \tag{47}$$

where $L = 1/\lambda$ for a simpler expression without compromising generality. Then, according to **Assumption 1**, **Lemmas 3**, and **5**, we rearrange the terms and take the average over t on both sides as follows:

$$\begin{aligned}\frac{1}{T}\sum_{t=1}^{T}\|\nabla \mathsf{F}(\mathbf{w}^t)\|_2^2 \le \frac{2(\mathsf{F}(\mathbf{w}^1) - \mathsf{F}(\mathbf{w}^\star))}{\lambda T} + \frac{\xi\sigma^2 G^2 \mathsf{E}_1(\delta)}{2P_0K^2} \\ + (1 + \xi e^{-\delta})G^2, \end{aligned} \tag{48}$$

which completes the proof. ∎

ACKNOWLEDGMENT

This work was supported in part by the IITP (Institute of Information & Communications Technology Planning & Evaluation) - ITRC (Information Technology Research Center) (IITP-2026-RS-2022-00156353, 50%) grant funded by the Korea government (Ministry of Science and ICT) and in part by the National Research Foundation of Korea (NRF) grant funded by the Korea government (MSIT) (No. RS-2023-00209125).

REFERENCES

[1] B. McMahan, E. Moore, D. Ramage, S. Hampson, and B. A. Y. Arcas, "Communication-efficient learning of deep networks from decentralized data," in *Proc. Artif. Intell. Statist. (AISTATS)*, Fort Lauderdale, FL, USA, Apr. 2017, pp. 1273–1282.

[2] D. Kwon, J. Jeon, S. Park, J. Kim, and S. Cho, "Multiagent DDPG-based deep learning for smart ocean federated learning IoT networks," *IEEE Internet Things J.*, vol. 7, no. 10, pp. 9895–9903, Oct. 2020.

[3] J. Bang, S. Woo, and J. Lee, "DRL-empowered joint batch size and weighted aggregation adjustment mechanism for federated learning on non-IID data," *ICT Express*, vol. 10, no. 4, pp. 863–870, Aug. 2024.

[4] D. C. Nguyen, M. Ding, P. N. Pathirana, A. Seneviratne, J. Li, and H. V. Poor, "Federated learning for internet of things: A comprehensive survey," *IEEE Commun. Surveys Tuts.*, vol. 23, no. 3, pp. 1622–1658, 3rd Quart. 2021.

[5] G. Zhu, Y. Wang, and K. Huang, "Broadband analog aggregation for low-latency federated edge learning," *IEEE Trans. Wireless Commun.*, vol. 19, no. 1, pp. 491–506, Jan. 2020.

[6] K. Yang, T. Jiang, Y. Shi, and Z. Ding, "Federated learning via over-the-air computation," *IEEE Trans. Wireless Commun.*, vol. 19, no. 3, pp. 2022–2035, Mar. 2020.

[7] G. Zhu, Y. Du, D. Gündüz, and K. Huang, "One-bit over-the-air aggregation for communication-efficient federated edge learning: Design and convergence analysis," *IEEE Trans. Wireless Commun.*, vol. 20, no. 3, pp. 2120–2135, Mar. 2021.

[8] X. Fan, Y. Wang, Y. Huo, and Z. Tian, "1-bit compressive sensing for efficient federated learning over the air," *IEEE Trans. Wireless Commun.*, vol. 22, no. 3, pp. 2139–2155, Mar. 2023.

[9] M. M. Amiri and D. Gündüz, "Federated learning over wireless fading channels," *IEEE Trans. Wireless Commun.*, vol. 19, no. 5, pp. 3546–3557, May 2020.

[10] X. Cao, G. Zhu, J. Xu, and S. Cui, "Transmission power control for over-the-air federated averaging at network edge," *IEEE J. Sel. Areas Commun.*, vol. 40, no. 5, pp. 1571–1586, May 2022.

[11] Y. Shao, D. Gündüz, and S. C. Liew, "Federated edge learning with misaligned over-the-air computation," *IEEE Trans. Wireless Commun.*, vol. 21, no. 6, pp. 3951–3964, Jun. 2022.

[12] Y. Liang, Q. Chen, G. Zhu, H. Jiang, Y. C. Eldar, and S. Cui, "Communication-and-energy efficient over-the-air federated learning," *IEEE Trans. Wireless Commun.*, vol. 24, no. 1, pp. 767–782, Jan. 2025.